N87-11213

# Oxidation and Low Cycle Fatigue Life Prediction

Yoshiki Oshida and Hao-Wen Liu
Department of Mechanical Engineering
Syracuse University

When a metallic material is exposed to a high temperature in an ambient atmosphere, oxidation takes place on the metallic surface. The formed oxides (both surface and grain boundary oxides) are mechanically brittle so that if the stress is high enough the oxides will be cracked. This oxide crack will become the nucleus of a fatigue crack if the allpied $\Delta J$ is larger than $\Delta J_{th}$. Therefore oxidation may reduce high temperature low cycle fatigue life.

## Grain Boundary Oxidation

The grain boundary oxide formation in TAZ-8A nickel-base superalloy was studied. The effect of oxide crack nucleus on low cycle fatigue life will be analyzed. TAZ-8A was subjected to high temperature oxidation tests in air under the stress-free condition. The oxidation temperatures were 600°, 800°, and 1000°C. The oxidation time varied from 10 to 1000 hours. The temperatures were controlled within ± 8°C.

Figure 1 shows the measured weight gain per unit area of exposure, $\Delta W$ [mg/cm$^2$] as a function of exposure time for three different test temperatures. If oxidation of TAZ-8A obeys the parabolic rate law, the square of $\Delta W$ should relate linearly to oxidation time as shown in figure 2. Many other superalloys and refractory materials have exhibited the parabolic rate law for oxidation. The parabolic oxidation rate indicates that oxidation is controlled by diffusion kinetics.

The slope of these straight lines is called parabolic rate constant, a. Figure 3 shows the relationship between parabolic rate constants and inverse absolute temperatures for a number of superalloys. TAZ-8A shows a superior oxidation resistance than Rene 41 and Mar-M200. The data seem to follow two line segments similar to Mar-M200. This change of the slope might be related to the change in diffusion mechanism. At the higher temperatures (i.e., between 800° and 1000°C), oxidation is mainly controlled by outward diffusion of Cr.

Grain boundary oxidation is faster and penetrates deeper. Therefore the grain boundary oxide cracks are larger and they are more critical in reducing the low cycle fatigue life. The oxidation rate was measured in terms of weight gain, and the oxidation penetration was measured by direct optical observation. One of the main objectives of the current research program is to separate the grain boundary oxidation from the total oxidation. The weight gain ($\Delta W_T$) was measured, and it is simply the sum of weight gain due to surface oxidation ($\Delta W_S$) and the weight gain due to grain boundary oxidation ($\Delta W_G$). $\Delta W_S$ and $\Delta W_G$ can be easily separated by calculating $\Delta W_S = V_S \times \rho_S$, where $V_S$ is the total volume of surface oxide layer of a test coupon, and $\rho_S$ is the specific gravity of surface oxides. The calculated results are shown in figure 4. This approach for separation of $\Delta W_S$ and $\Delta W_G$ is based on the assumption of homogeneous surface oxide layer thickness.

A second way to separate $\Delta W_S$ and $\Delta W_G$ is by calculating weight gain due to grain boundary oxidation by morphological measurements of width (GPW) and depth (GPD) of grain boundary oxide penetration. Figure 5 is one example of the results of this morphological study on oxidized coupon (1000°C x 960 hr). The shape of grain boundary oxides can be classified into two groups (round-edge and sharp-edge). This figure shows the size as well as the shape of the grain boundary oxides. The frequencies of the observed oxide size and shape are indicated by the size and shape of the data points in the figure. The data have considerable scatter in the GPW vs. GPD relationships. Based on the morphological analysis that the average value of the aspect ratio (GPW/GPD) of grain boundary oxides is close to 1.0; so only the data point on the 45 degree dashed line are used for calculation of grain boundary oxide weight. Each of the numbers on the 45 degree dashed line is the percentage of the number of the data points for the

morphology over the total number of all of the data points along this dashed line. Let us call these numbers as distribution percentage, $p_i$. The weight gain due to grain boundary oxidation ($\Delta W_G$) can be estimated as

$$\Delta W_G = N \times \rho_{GO} \times \sum_{i=1}^{n} V_{GOi} \times p_i$$

where $V_{GOi}$ is the volume of grain boundary oxide per grain at the ith morphology in figure 5, $\sum_{i=1}^{n} V_{GOi} \times p_i$ is the average volume of grain boundary oxide per grain

N is the total number of grains on the surface of the test coupon which was obtained as the total surface area of a coupon divided by average grain size area, and $\rho_{GO}$ is the specific gravity of grain boundary oxides which is assumed to be equal to $\rho_S$. $V_{GOi}$ can be calculated from the GPW, GPD, and the shape. The calculated results of $\Delta W_G$ and $\Delta W_S$ (= $\Delta W_T$ - $\Delta W_G$) based on this morphological approach are also plotted in figure 4. Except in the early stage of oxidation, both approaches for separation of grain boundary oxidation from total oxidation are satisfactory.

Figure 6 shows both the calculated results of $\Delta W_G$ according to the surface homogeneous oxide layer and $\Delta W_G$ based on the morphological approach for grain boundary oxides at three different oxidation temperatures. These two measurements agree reasonably well with each other.

In figure 7, the data on total oxidation are exactly the same as those shown in figure 3. Of interest is that (i) grain boundary oxidation rate, in terms of its parabolic rate constant, is $10^2$ time larger than the total oxidation and the surface oxidation, and (ii) in both grain boundary and surface oxidation, the similar breaking points at 800°C were found as that for the total oxidation.

The application of the statistical theory of extreme values to the analysis of maximum pit depth due to pitting corrosion was successfully introduced by Aziz (ref.1) and Hawn (ref.2). For some high temperature alloys, low cycle fatigue (LCF) cracks at elevated temperatures were often initiated as grain boundary oxides, and the maximum grain boundary oxide depth will control the LCF crack initiation period as well as the early stage of crack propagation period. Therefore the most important measure of "damage" to a specimen is grain boundary oxide penetration depth. This is analogous to the maximum pit depth of Aziz (ref.1). Aziz found that the maximum pit depth obeys the Poisson's distribution. The oxidized coupons were sectioned, and the cross sectional surface was examined under an optical microscope and the maximum grain boundary oxide penetration depth, $a_o$, of this surface was recorded. After approximately 50 μm of the surface layer was removed another maximum $a_o$ was recorded. A coupon was machined and examined repeatedly layer after layer. All together 12 data points were collected for each of the three coupons oxidized at different temperatures. Assuming a Poisson's distribution, figure 8 shows the results for 800°C oxidation temperature at four different oxidation times. The straight lines are drawn by the least square fit. Suppose the surface area ratio of a real component to the test coupon is 100, the extrapolated $a_o$ value can be read on the line at the return period = 100. For example in the case of 800°C x 960 hr oxidation, on the small test coupon area, the deepest $a_o$ is 120 μm, whereas on a surface area 100 times larger, the likely $a_o$ is 158 μm. According to Aziz(ref.1), "rather than considering the return period, it is equally worthwhile to consider the frequencies" on the left side of the figure. The probability of obtaining an $a_o$ of 158 μm is 0.990. Therefore there is only one chance in a hundred to have $a_o$ deeper than 158 μm on the total surface area of the 12 layers of the tested coupon oxidized at 800°C for 960 hrs. This should be equivalent to the test of 12 sectioned surfaces of 12 separate coupons.

Because of the brittle property of oxides, a crack might be initiated at a grain boundary oxide. Once a crack is initiated and if the applied cyclic stress is high enough, the crack will propagate by the fatigue loading. Therefore the grain boundary oxides can be considered as a crack nucleus. It is reasonable to expect that the rates of both surface oxidation and grain boundary oxidation will be accelerated by mechanical stress, and that the grain boundary oxide penetration depth will be increased by a high enough applied stress.

## Grain Boundary Oxide Crack and Low Cycle Fatigue Life - A Preliminary Analysis

Fatigue life consists of crack nucleation and crack propagation periods. Fatigue crack nucleation period is relatively shorter at higher stresses. Low cycle fatigue crack nucleation period might even be shortened by severe environmental attack, such as oxidation. In this case, fatigue life consists mainly of crack propagation period.

For general-yielding cyclic-loading, Dowling and Begley (ref.3) have shown that fatigue crack growth rate correlates well with $\Delta J$; and near the threshold, da/dN can be written in the form (ref.4 and 5).

$$\frac{da}{dN} = A \frac{\Delta J_{th}}{\sigma_{YC}} \left( \frac{\Delta J}{\Delta J_{th}} - 1 \right)^m \tag{1}$$

Zheng and Liu (ref.5) have shown that for a small crack in a large solid,

$$J = [\eta_1 DW + \eta_2 \sigma_Y \varepsilon_Y] a \tag{2}$$

DW is deformation work density. For cyclic loading, it is related to the applied stress and strain ranges.

$$DW = [\frac{\Delta\sigma^2}{8E} + \sigma_{YC} \Delta\varepsilon_p] \tag{3a}$$

$$= \alpha [\frac{\Delta\sigma}{2} (\Delta\varepsilon_p + \frac{\Delta\varepsilon_e}{2})] \tag{3b}$$

where $\Delta\sigma$, $\Delta\varepsilon_e$, and $\Delta\varepsilon_p$ are the applied stress, elastic strain, and plastic strain ranges. E and $\sigma_{YC}$ are Young's modulus and cyclic yield strength.

Fatigue life can be obtained by integrating equation (1) (ref.5).

$$(DW)^m N_f = \frac{\sigma_{YC}}{A(m-1)\eta_1^m} \left( \frac{\Delta J_{th}}{a_i} \right)^m - 1$$

$$= C\, a_i^{(1-m)} \tag{4}$$

where $a_i$ is the crack nucleus size. Fatigue life, $N_f$ is related to the size of the crack nucleus $a_i$.

Figures 9 and 10 show the correlations of low cycle fatigue lives of an aluminum alloy with these two parameters of deformation work density (equations 3a and 3b). In figures 9 and 10, fatigue lives of both smooth and pre-cracked specimens are plotted. The size of the pre-cracks, $a_o$ is larger than $a_i$. According to eq.(4), the fatigue lives of the smooth and the pre-cracked specimens ($N_f$ and $N_{fo}$) are related.

$$\frac{N_{fo}}{N_f} = \left( \frac{a_o}{a_i} \right)^{1-m} = \text{constant} \tag{5}$$

Therefore, the log-log plots of the fatigue lives of the smooth and pre-cracked specimens are parallel as shown in figures 9 and 10.

The grain boundary oxide cracks can be considered as pre-cracks. Therefore the fatigue lives of oxidized specimens will have a similar relation.

As shown by the data in figures 5 and 8, the oxide crack size may have a substantial statistical scatter; and it is expected that this statistical scatter will be reflected in the fatigue lives of the oxidized specimens.

It should be emphasized that the analysis on the fatigue lives of oxidized specimens is preliminary. However, it can serve as the guide for the future study.

References


(1) P.M.Aziz; Corrosion, 12(10), 1956, pp.495A-506A.
(2) D.E.Hawn; Materials Performance, 1977, pp.29-32.
(3) N.E.Dowling and J.A.Begley; ASTM STP Vol.590, 1976, pp.80-103.
(4) H.W.Liu and Dai Liu; Scripta Met., 18, 1984, pp.7-12.
(5) M.Zheng and H.W.Liu; Technical Report NASA Grant No. NAG3-348 "Crack Tip Field and Fatigue Crack Growth in General Yielding and Low Cycle Fatigue", 1984.


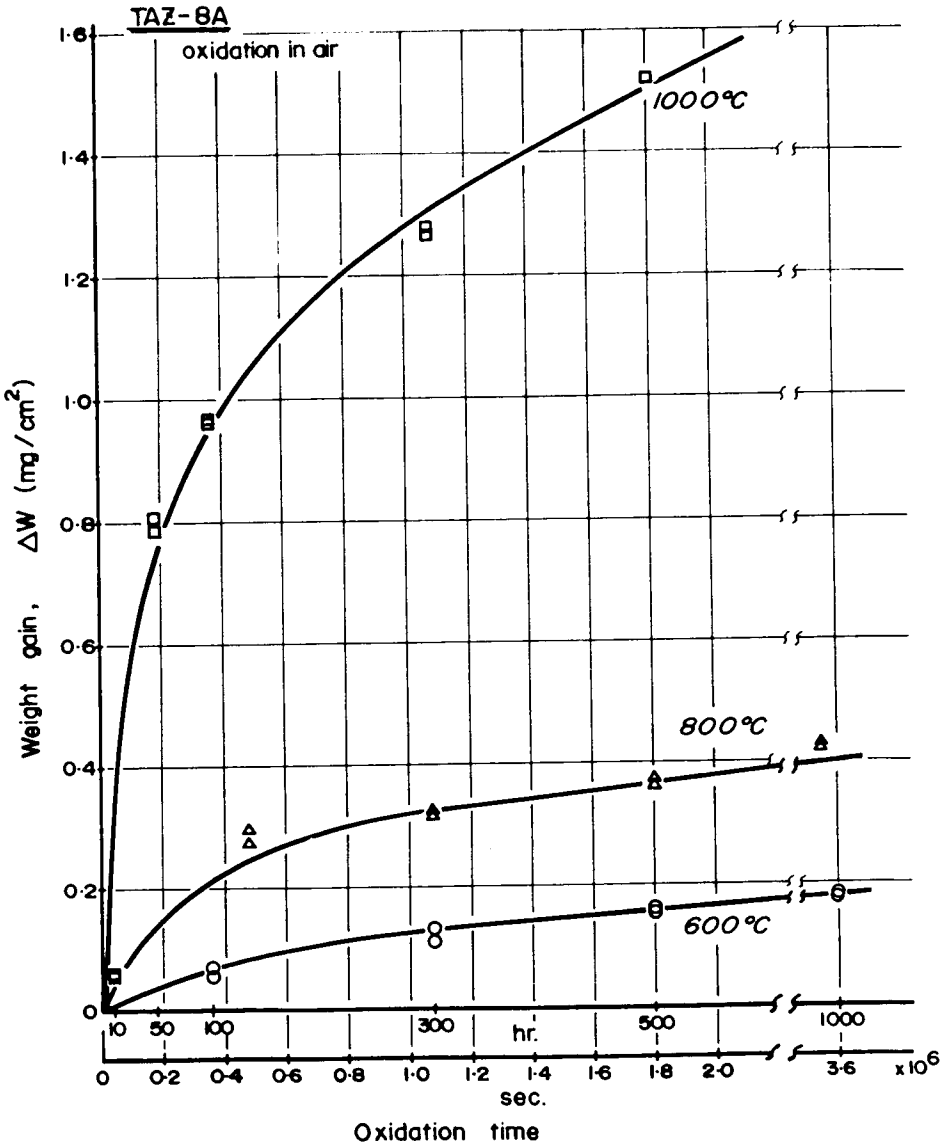


Fig. 1 Total weight gain vs. oxidation time

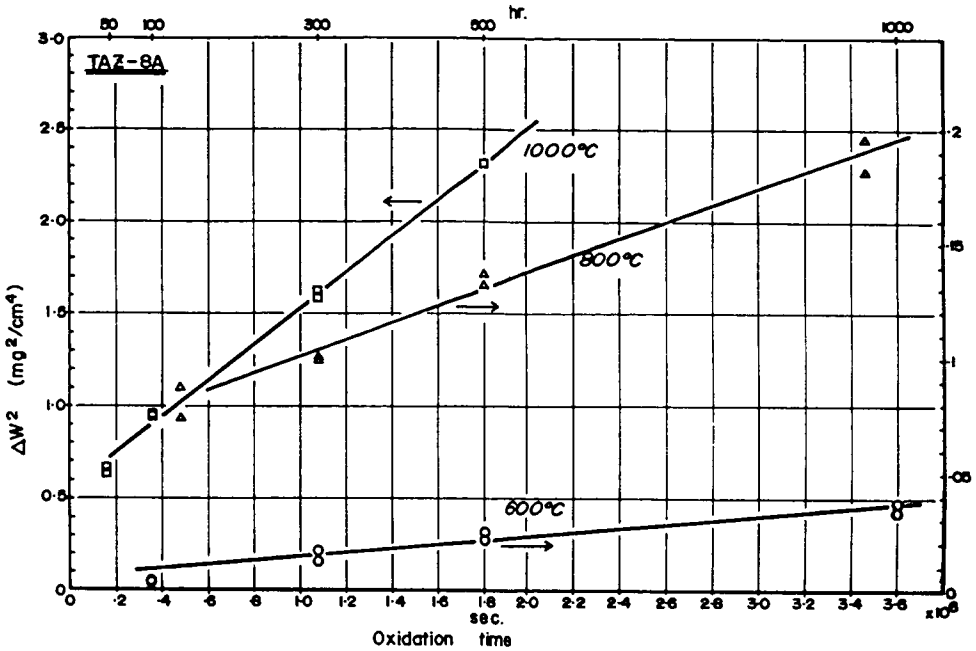


Fig. 2 Square of total weight gain vs. oxidation time

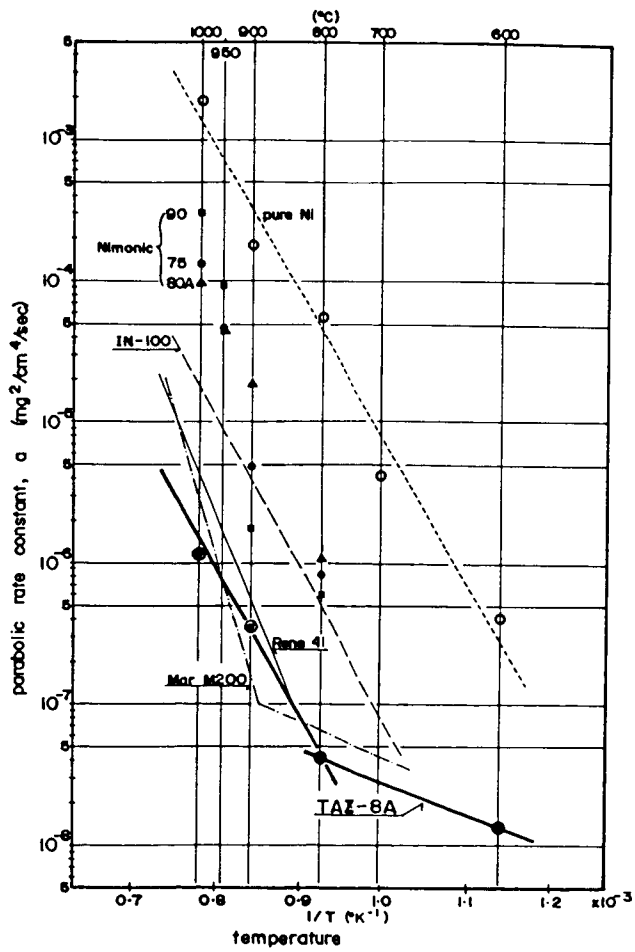


Fig. 3 Parabolic rate constant vs. inverse absolute temperature

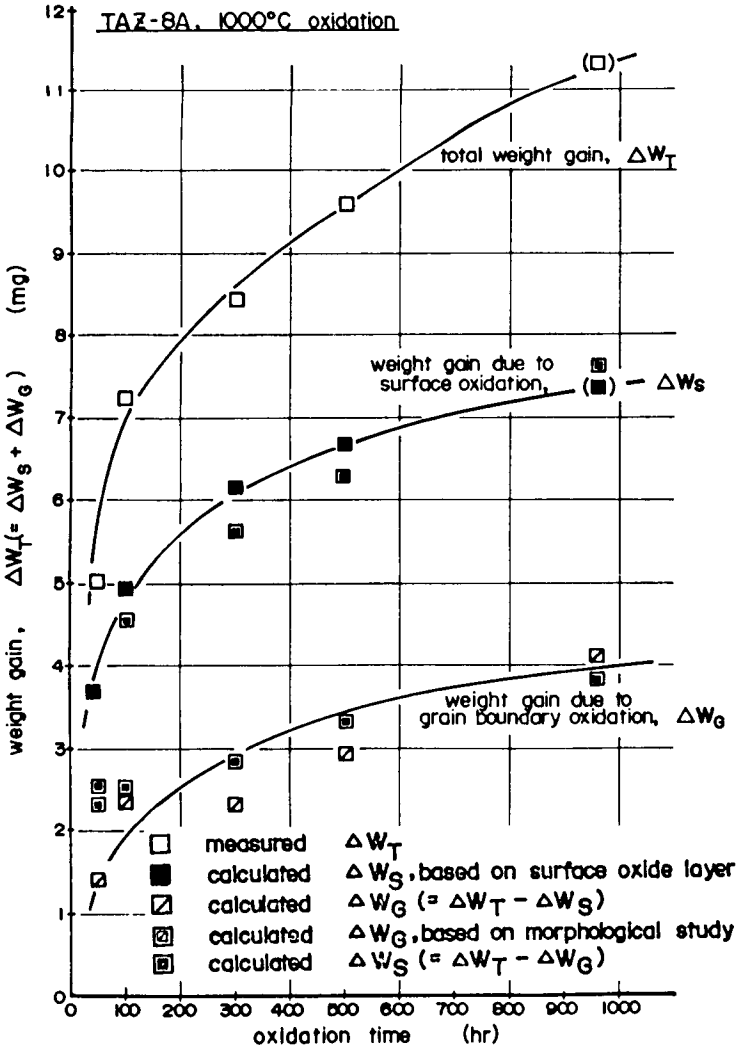


Fig. 4 Weight gain (total, surface oxidation, and grain boundary oxidation) vs. oxidation time

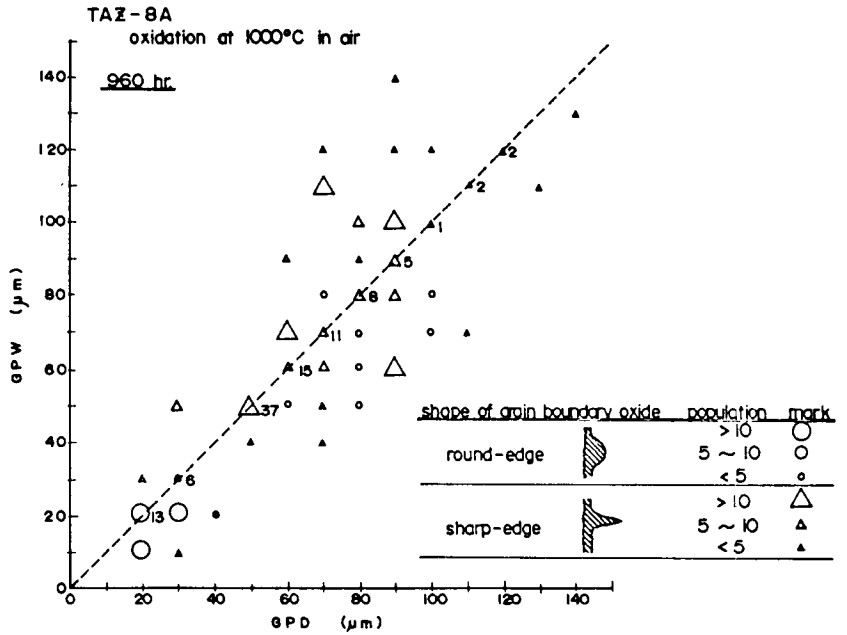


Fig. 5 Results of morphological study on grain boundary oxide

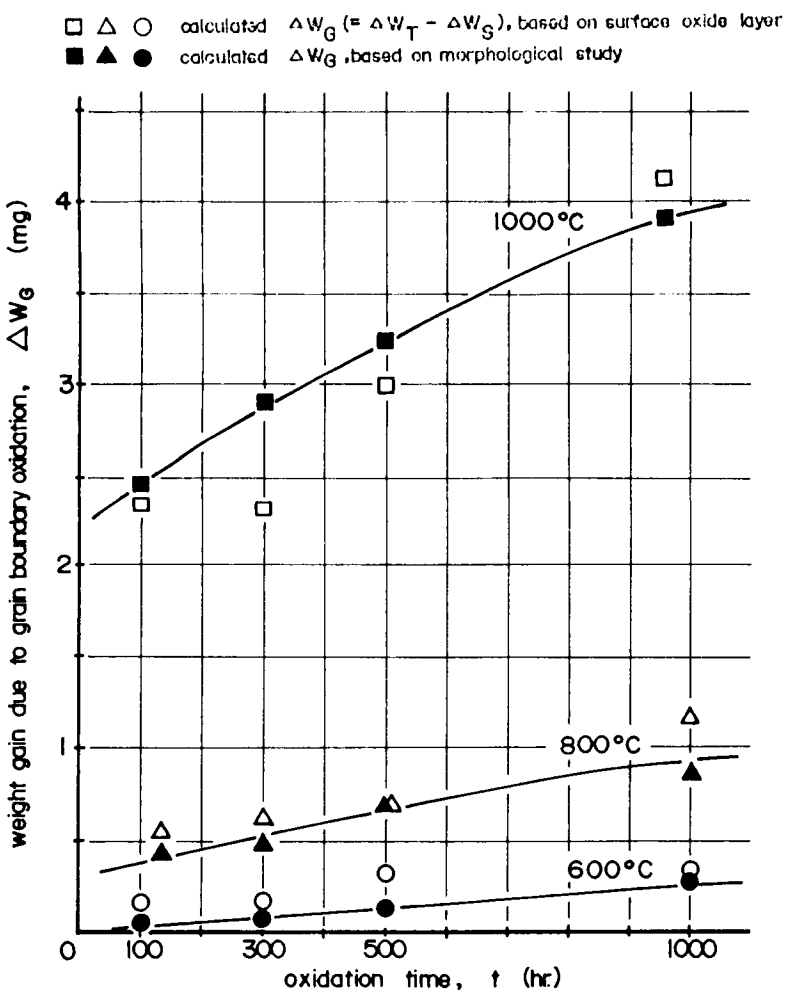


Fig. 6 Weight gain due to grain boundary oxidation vs. time

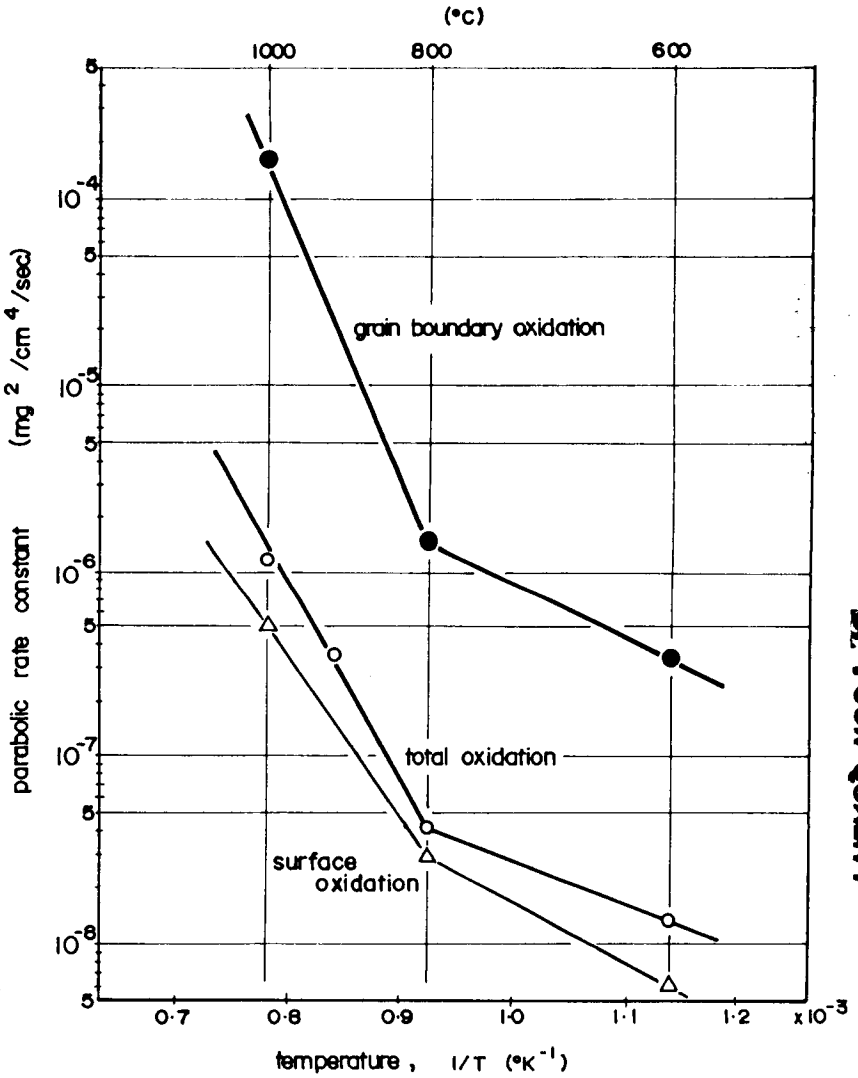


Fig. 7 Parabolic rate constants of total oxidation and grain boundary oxidation vs. inverse absolute temperature

ORIGINAL PAGE IS
OF POOR QUALITY

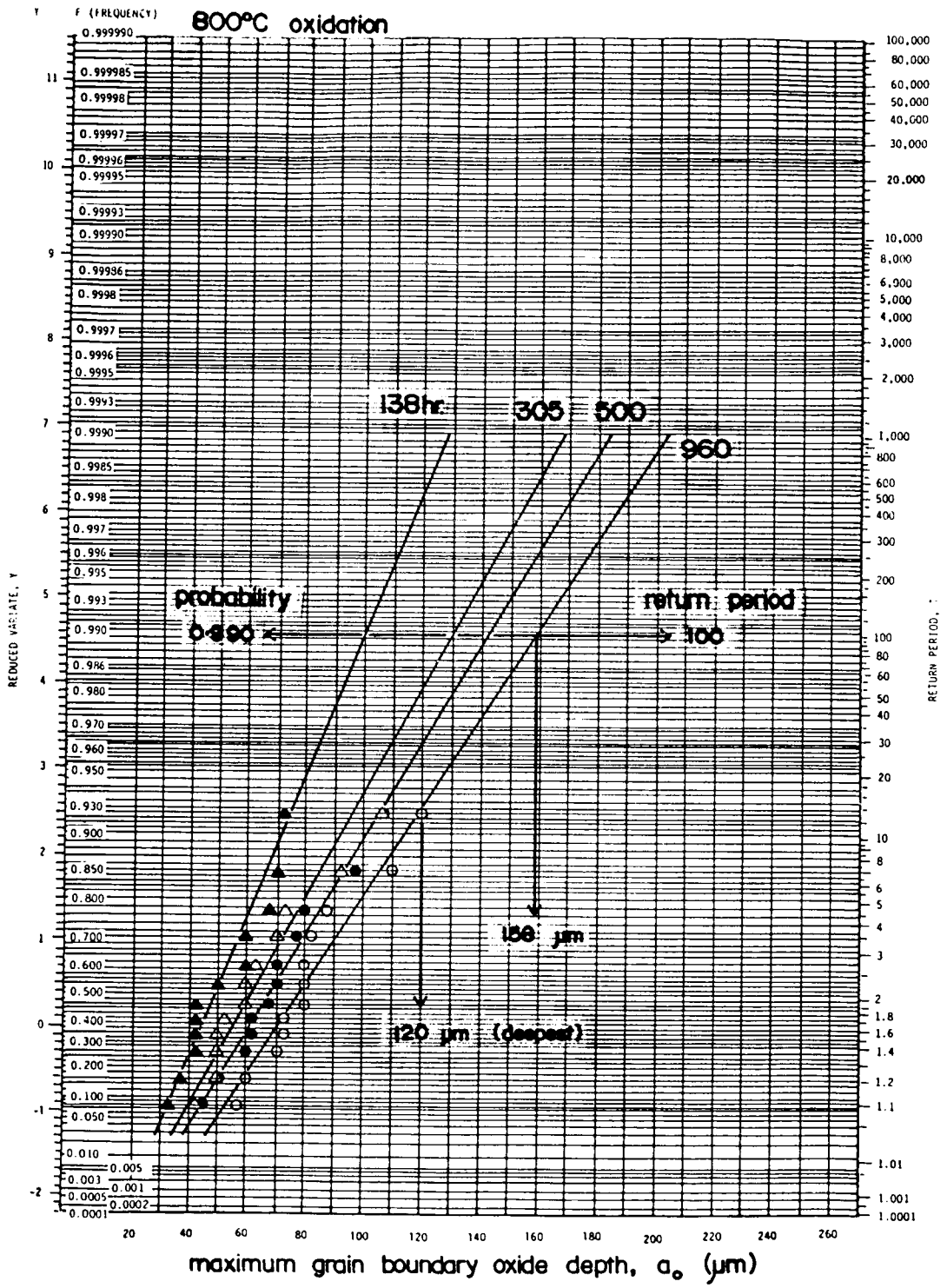


Fig. 8 Maximum grain boundary oxide depth vs. frequencies

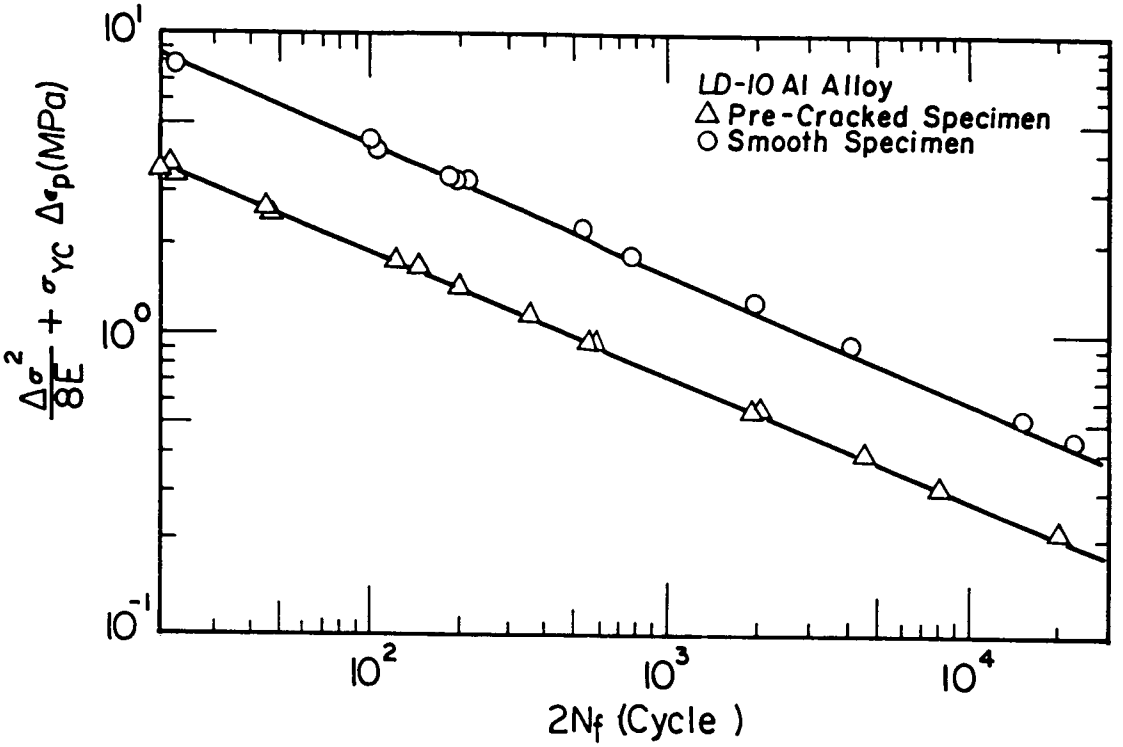


Fig. 9 Correlation of $(\frac{\Delta\sigma^2}{8E} + \sigma_{YC}\Delta\varepsilon_p)$ versus $(2N_f)$ for LD-10 aluminum alloy.

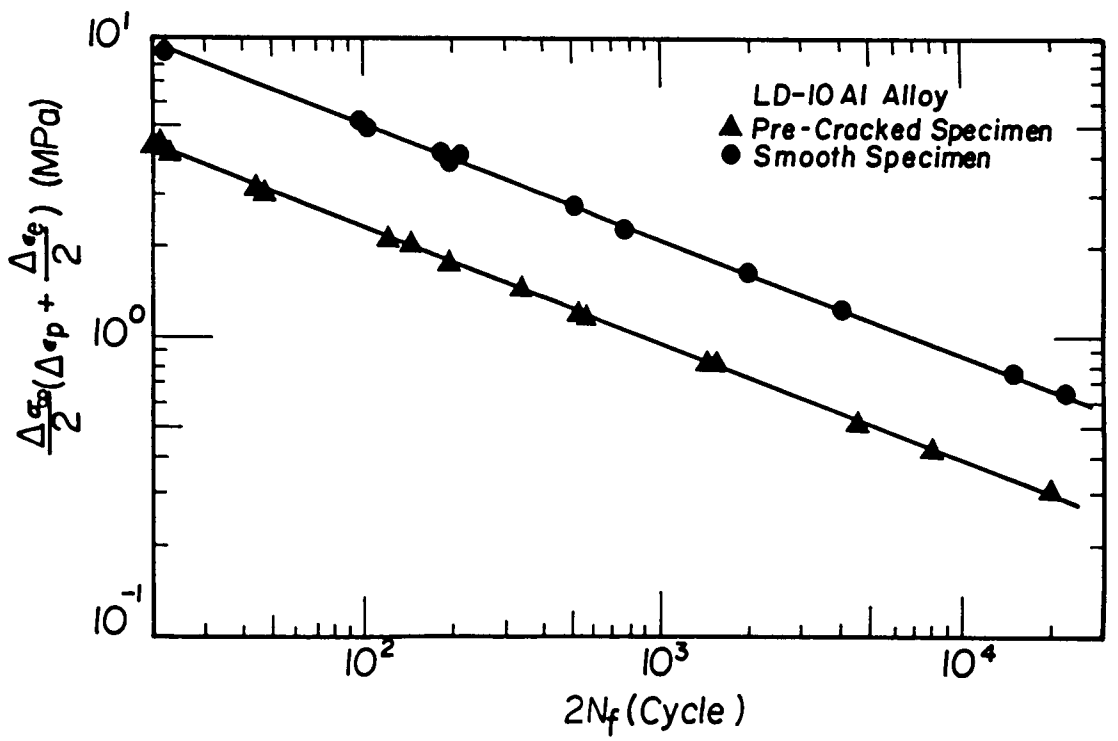


Fig. 10 Correlation of $[\frac{\Delta\sigma_\infty}{2}(\Delta\varepsilon_p + \frac{\Delta\varepsilon_e}{2})]$ versus $(2N_f)$ for LD-10 aluminum alloy.